# First-principles based thermodynamic model of phase equilibria in bcc Fe-Cr alloys

A. V. Ruban and V. I. Razumovskiy*

*Department of Materials Science and Engineering, Royal Institute of Technology, SE-100 44 Stockholm, Sweden*

(Received 21 November 2011; revised manuscript received 29 August 2012; published 15 November 2012)

A first-principles based thermodynamic model for magnetic alloys is applied to the calculation of the Fe-Cr phase diagram restricted by the bcc structure. The model includes magnetic, electronic, phonon, and local atomic relaxations contributions to the free-energy derived from *ab initio* calculations. Atomic short-range-order effects are found to be relatively small and they have been neglected in the calculations, assuming that alloys are in the completely random state. In contrast, we have taken into consideration magnetic short-range-order effects, which are found to be very important in particular above the Curie temperature. The calculated phase diagram is in reasonable agreement with the latest CALPHAD assessment. Our calculations reproduce a feature known as a Nishizawa horn for the Fe-rich high-temperature part of the phase diagram.

DOI: 10.1103/PhysRevB.86.174111 PACS number(s): 31.15.A−, 81.30.Bx, 75.50.Bb

## I. INTRODUCTION

Understanding phase equilibria in Fe alloys is of great importance for materials science and solid state physics as well as for the development of high-performance steels. In particular, bcc Fe-Cr alloys have lately become a subject of intensive investigations due to their potential applications as construction materials for nuclear fission and fusion reactors.[1] According to the existing data[2] the phase diagram of the bcc Fe-Cr system is quite simple: The bcc solid solution undergoes a decomposition onto the mixture of Cr-rich and Fe-rich alloys at temperatures below about 750 K. However, the experimental data on the phase boundaries are rather scattered.[3] The data by Dubiel and Inden,[4] based on the samples of Fe-Cr alloy annealed up to 11 years, can be considered as the closest to the thermal equilibrium, but they are only for a very narrow temperature range from 733 to 783 K.

Different empirical models have been used in phase diagram calculations of Fe-Cr alloys.[5,6] In this case, the CALPHAD method[7] has an advantage due to direct modeling of the Gibbs free-energy based on the known experimental information about thermodynamic properties of the system and phase equilibria. Xiong *et al.*[3] have recently performed a comprehensive CALPHAD investigation of the Fe-Cr system, and bcc Fe-Cr alloys in particular, and introduced a new CALPHAD description, which is supposed to replace the commonly accepted one by Andersson and Sundman.[7] As have been noted by Xiong *et al.*,[3] "... In spite of numerous experiments, the determined location of the metastable bcc miscibility gap is still ambiguous, especially for the critical solution temperature of the miscibility gap."

It is clear that the existing phenomenological theories of Fe-Cr alloys, closely or directly related to the CALPHAD method, can provide a detailed and accurate description of phase equilibria in this system only under the condition if there exist reliable experimental data for a wide range of temperatures and concentrations, which is not the case here. The other problem of the CALPHAD-type methods is the fact that they do not disclose the driving forces behind phase equilibria at the atomic or electronic structure levels. The latter are needed for effective intelligent design of new materials, when the experimental data are not available.

Such information can be only obtained by methods based on first-principles electronic structure calculations. Unfortunately, the existing first-principles calculations of the Fe-Cr phase diagram suffer from the incorrect account of the magnetic state. In the earlier work by Turchi *et al.*[8] the phase diagram was calculated using effective pair interactions of an Ising Hamiltonian determined in the calculations of *nonmagnetic* Fe-Cr alloys. At the same time, according to the existing phase diagram, the phase boundary of the Fe-rich alloys is *below* the magnetic phase transition, that is, these alloys are in the ferromagnetic state. The other work by Lavrentiev *et al.*[9] uses the opposite assumption, considering everything in the totally ordered ferromagnetic state, which corresponds to the zero temperature, even in the case when the authors consider phase equilibrium at temperatures far above the magnetic phase transition.

Recently, Lavrentiev *et al.*[10] developed a microscopic phenomenological model, the so-called magnetic cluster expansion, which made possible a consideration of the finite-temperature magnetic excitations in the phase equilibria calculations. The parameters of the Hamiltonian were fitted to the *ab initio* calculations of some FeCr structures. This model Hamiltonian was then used to investigate the polymorphous high-temperature transformation in pure Fe and the so-called $\gamma$ loop in the Fe-Cr alloys. Although such a consideration looks promising, it cannot be used at low temperatures, where quantum mechanical effects are important. Besides, it is not clear how to use this formalism for the description of the phase separation, where the knowledge of the Gibbs free-energy is needed.

In fact, the importance of magnetism for the thermodynamics of Fe and its alloys was recognized a long time ago.[11,12] As far as the Fe-Cr system is concerned, the impact of the magnetic state upon thermodynamic properties of Fe-Cr alloys has been clearly demonstrated in a number of recent first-principles investigations.[13–16] In particular, the enthalpies of formation of random Fe-Cr alloys differ substantially in the ferromagnetic and paramagnetic states.[13,14,16]

As has been shown in Ref. 17, even a small deviation of the global magnetization from the saturated magnitude leads to a substantial change of the effective chemical interactions, which exhibit quite strong concentration dependence[17–20] also

 

directly connected to the magnetism and magnetic state of Cr atoms in particular.[17] Such an anomalous alloying behavior is observed in the Fe-rich alloys in a rather narrow temperature range of 600–900 K. This is the most important region from a technological point of view and, as a matter of fact, the most difficult one for accurate and reliable theoretical description.

In this paper we present a first-principles-based thermodynamic investigation of phase equilibria in bcc Fe-Cr alloys. It incorporates a number of models for different contributions to the Gibbs free-energy. The first-principles results, which are used for modeling, are obtained by the state-of-the-art density functional theory (DFT) methods. Since the latter cannot be directly used in the calculations of the thermodynamic properties related to the finite temperature magnetic excitations, we use different models for the magnetic energy below as well as above the Curie temperature.

The use of such models is of a practical necessity since an accurate account of finite temperature magnetism in itinerant systems is only possible in *ab initio* methods going beyond DFT. Although our final results are not truly *ab initio*, we believe that they provide a valuable insight into the driving forces behind phase equilibria in Fe-Cr alloys and may be helpful in improving thermodynamic modeling in the CALPHAD-type methods. Besides, they allow one to identify the weakest and most difficult points in the first-principles modeling.

## II. DETAILS OF FIRST-PRINCIPLES CALCULATIONS

### A. Full charge density exact muffin-tin orbital method calculations

Electronic structure calculations of Fe-Cr alloys have been mainly performed by means of the exact muffin-tin orbitals (EMTO) method[21–24] within the framework of DFT.[25] Substitutional disorder has been treated by using the coherent potential approximation (CPA).[26] The applicability of the CPA to the electronic structure calculations of Fe-Cr alloys has been checked in supercell calculations[16,27,28] by *ab initio* different techniques including the locally self-consistent Green's function (LSGF) method within the EMTO formalism.[29,30] In particular, such calculations have been used to determine the contributions from the screened Coulomb interactions to the one-electron potential $V_i^{\rm scr}$ of alloy components $i$, and the total energy $E_{\rm scr}$, within the single-site DFT formalism:[31]

$$V_i^{\rm scr} = -\alpha \frac{e^2 q_i}{S} \quad \text{and} \quad E_{\rm scr} = \frac{\beta}{2} \sum_i c_i q_i V_i^{\rm scr}. \qquad (1)$$

Here $e$ is the electron charge, $S$ is the Wigner-Seitz radius, and $q_i$ and $c_i$ are the average net charge of the atomic sphere and the concentration for the $i$th alloy component, respectively. The values of $\beta$ were found to vary linearly from $\beta = 1.00$ to $\beta = 1.14$, and those of $\alpha$ parameter to vary nonlinearly from $\alpha = 0.658$ to $\alpha = 0.830$, as the alloy concentration changes from 0 to 100 at.% Cr. Note that the screened Coulomb interactions are treated quite arbitrarily in the similar EMTO-CPA calculations in Refs. 13 and 14, which may result in an inaccurate description of the thermodynamic properties.

The total energies were determined using the generalized gradient approximation[32] (GGA) within the full charge density (FCD) formalism.[24] All the self-consistent EMTO-CPA calculations were performed by using an orbital momentum cutoff of $l_{\rm max} = 3$ for partial waves. The integration over the Brillouin zone was done using a $31\times31\times31$ grid of **k** points determined according to the Monkhorst-Pack scheme[33] in all the EMTO calculations except those for the exchange interaction parameters. In the latter case, the Monkhorst-Pack grid was $55\times55\times55$. The core states were recalculated at each self-consistency iteration.

The CPA was also employed for modeling the paramagnetic state within the disordered local moment (DLM) model.[34,35] In this model each alloy component is presented by its spin-up ($\uparrow$) and spin-down ($\downarrow$) counterparts assumed to be distributed randomly on the underlying lattice. The ferromagnetic state with reduced magnetization $m$, due to thermal disorder of spin orientation, has been described by the partially disordered local moment (PDLM) model adopted in Ref. 17, where a binary $Fe_cCr_{1-c}$ alloy was presented by a random ternary alloy $(Fe_x^{\uparrow}\ Fe_{1-x}^{\downarrow})_cCr_{1-c}$, where

$$x = \frac{m+1}{2}. \qquad (2)$$

Note that in the FM and PDLM calculations, the local magnetic moment of Cr atoms was relaxed to its equilibrium magnitude and in most of the cases it was antiparallel to that of Fe.[13–16,36] Equilibrium Wigner-Seitz radii (or equivalently, lattice constants), bulk moduli, and their volume derivatives have been determined by fitting the total energies of Fe-Cr alloys by the third order polynomials in the Wigner-Seitz radii interval from 2.58 to 2.70 a.u. with step 0.01 a.u. at each concentration (from 0 to 30 at.% Cr with step 2%, from 30 to 100 at.% Cr with step 10%) with specific magnetization (from 1 to 0.6 with step 0.04, from 0.6 to 0 with step 0.2). In total, more than 4000 self-consistent EMTO-CPA calculations have been done in order to get the needed thermodynamic functions.

### B. Projector augmented wave method calculations

We have also used the full potential projector augmented wave (PAW) method[37,38] as implemented in the Vienna *ab initio* simulation package (VASP).[39–41] In particular, the PAW method was used to calculate electronic structure, equilibrium volume, and local lattice relaxations in random $Fe_{0.9375}Cr_{0.0625}$, $Fe_{0.875}Cr_{0.125}$, $Fe_{0.75}Cr_{0.25}$, $Fe_{0.50}Cr_{0.50}$, $Fe_{0.75}Cr_{0.25}$, $Fe_{0.875}Cr_{0.125}$ alloys. These alloys were modeled by supercells of different sizes. In particular, a 128-atom supercell formed by $4\times4\times4$ translations of a two-atom ($\times2$) cubic unit cell of the bcc structure was used in calculations of $Fe_{0.875}Cr_{0.125}$, $Fe_{0.75}Cr_{0.25}$, $Fe_{0.50}Cr_{0.50}$, $Fe_{0.75}Cr_{0.25}$, $Fe_{0.875}Cr_{0.125}$ alloys. A larger, 256-atom supercell $[4\times4\times8(\times2)]$ was used to model the random $Fe_{0.9375}Cr_{0.0625}$ alloy, while the equiatomic random alloy $Fe_{0.5}Cr_{0.5}$ was represented by a 64-atom supercell ($4\times4\times4$) built upon a bcc primitive unit cell.

Accordingly, we have used the $4\times4\times4$ Monkhorst-Pack $k$-point mesh in the 128-atom and 64-atom supercell calculations and the $4\times4\times2$ $k$-point mesh in the case of the 256-atom supercell. The convergence with respect to the number of $k$ points has been checked by comparing the results for the equilibrium lattice constant and elastic moduli of 128-atom

supercell obtained using 2×2×2 and 4×4×4 $k$-point meshes. In order to keep the cubic symmetry of the underlying bcc lattice, which is preserved on average in real alloys, the shape of the unit cells was kept fixed while all the atomic positions inside the supercell were relaxed until the forces acting on atoms were less than $10^{-2}$ eV/Å. The GGA[32] has been used in the PAW self-consistent calculations. The convergence criterion for the total energy was $10^{-5}$ eV.

The total energies of pure elements in the PAW calculations of the enthalpies of formation of a particular alloy have been obtained by using the same supercells and parameters of the PAW method as in the total energy calculations of the corresponding alloy. This is necessary in order to avoid systematic errors.

The VASP-PAW method has been also used in the force-constant calculations, which have been done by the small-displacement method in a way similar to that described in Ref. 42 and as implemented in PHON[43,44] code. A force-constant (FC) model for a dilute limit is described in Sec. V C. We used a 64-atom supercell with 6×6×6 Monkhorst-Pack $k$-point mesh. The displacement amplitude was 0.04 Å. The convergence criterion was $10^{-8}$ eV for the total energy and $10^{-4}$ eV/Å for forces. The VASP-PAW force constant calculations were performed in the GGA.[45] The energy cutoff was 350 eV in all the VASP-PAW calculations.

## III. GROUND STATE PROPERTIES OF Fe-Cr ALLOYS

### A. Lattice constants

The lattice constants of random Fe-Cr alloys have been previously obtained theoretically at 0 K in the FM state in a number of EMTO-CPA calculations.[13,14,28,46] The present EMTO-CPA results are practically the same. They are shown in Fig. 1 together with our PAW supercell results for the whole concentration range and some experimental data.[47–50] In particular, we show the room-temperature data by Preston *et al.*,[47] the high-temperature (1200 K) data by Babyuk *et al.*,[49] and low-temperature data by Kohlhaas *et al.*[48] for bcc Fe and Sumin *et al.*[50] for Fe-rich alloys (other experimental data are not shown since they are very close to those presented in the figure).

First of all, one can see that the experimental lattice parameters are noticeably higher than the theoretical ones calculated at 0 K. In fact, this difference is mainly due to the errors in the description of the exchange-correlation part of the GGA total energy functional. Indeed, the experimental 0 K lattice parameter for Fe, with the contribution from the zero-point vibrations removed, is 2.853 Å,[51] while the corresponding theoretical values are noticeably smaller: 2.837 Å (EMTO), 2.833 Å (full-potential linearized augmented plane-wave plus local-orbitals method, Ref. 51), and 2.832 Å (VASP-PAW, this study).

Second, the zero-temperature FM theoretical and the room-temperature experimental lattice parameters exhibit substantially different concentration dependencies. In particular, the theory predicts a pronounced maximum at about 8 at.% Cr. This maximum has also been obtained in the previous EMTO-CPA calculations[13,16,28,46] as well as in the supercell PAW[28] and LSGF-EMTO calculations.[30] The origin of the difference between theory and experiment is not clear. It might be attributed, for instance, to atomic short-range order[30] in real alloys not accounted for in our calculations as well as to some temperature-dependent anomalies of the thermal lattice expansion. Let us note that to resolve this issue one needs to now not only alloy composition but also atomic configuration, which is practically impossible to deduce from the experimental papers. Let us note that the existing experimental low-temperature data for the lattice parameter of Fe (2.861 Å)[48] and $Fe_{0.88}Cr_{0.12}$ alloy (2.869 Å)[50] show approximately the same increase of the lattice parameter for this concentration interval (0.0077 Å) as theoretical results (0.009 Å).

Our calculations also predict the existence of a peculiar temperature and concentration behavior of the lattice constants in Fe-rich Fe-Cr alloys in the ferromagnetic state at low temperatures. In Fig. 2 we show the theoretical lattice parameter of

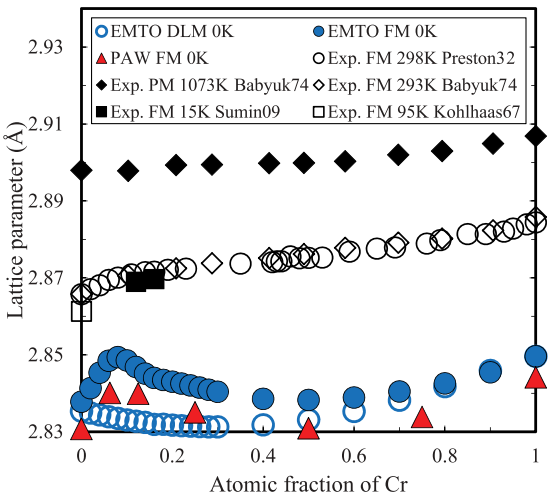


FIG. 1. (Color online) Calculated and experimental[47–50] lattice constants of Fe-Cr alloys. The EMTO results are obtained using the CPA. In the PAW calculations, alloys are modeled by supercells of different sizes.

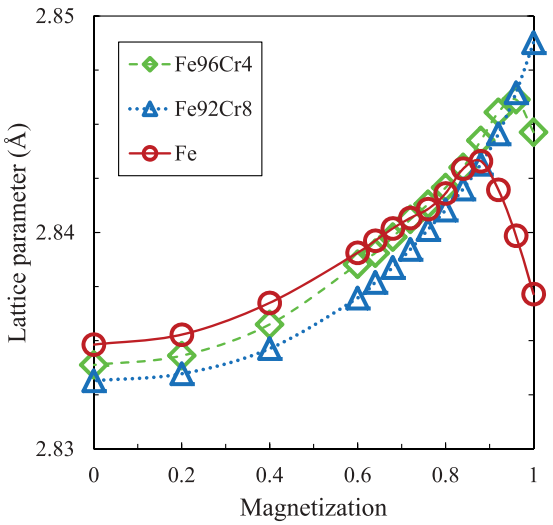


FIG. 2. (Color online) Calculated zero-temperature lattice constants for the Fe-rich Fe-Cr alloys as a function of magnetization for three different compositions.

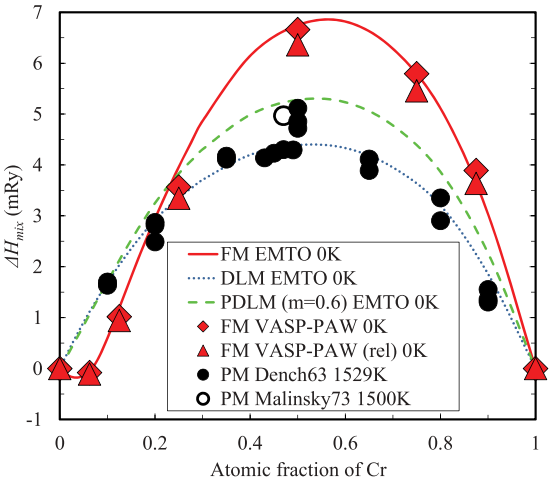


FIG. 3. (Color online) Theoretical enthalpies of mixing at 0 K and high-temperature experimental data[55,56] for the enthalpies of formation of bcc Fe-Cr alloys. The EMTO-CPA calculations are shown by solid (FM), dashed (PDLM for $m = 0.6$), and dotted (DLM) lines. The FM PAW results are shown by filled diamonds (unrelaxed) and triangles (relaxed).

pure Fe, and two alloys containing 4 and 8 at.% Cr, as a function of magnetization, which has been obtained in the EMTO-CPA calculations using the PDLM model as described above. In the case of $Fe_{0.92}Cr_{0.08}$, the lattice parameter increases with increasing magnetization, which is the expected behavior for an itinerant ferromagnet due to higher magnitude of the local magnetic moment in the FM state. However, the case of pure Fe is quite different: A pronounced maximum is observed at $m \approx 0.8$. Independently of the used model (PDLM), these results indicate that there can exist certain peculiarities in the temperature and concentration dependence of the lattice spacing of Fe-rich Fe-Cr alloys, which should be further investigated.

### B. Zero-temperature enthalpy of mixing

Zero-temperature enthalpy of formation of random Fe-Cr alloys has been determined and discussed in a large number of *ab initio* calculations.[9,13–16,52–54] In Fig. 3 we show the enthalpy of mixing of Fe-Cr alloys obtained in the EMTO-CPA calculations for three different magnetizations, $m = 1, 0.6$, and 0, using nonmagnetic Cr as a reference state. Our results for the FM ($m = 1$) and DLM ($m = 0$) states are practically the same as were reported in Ref. 16. The enthalpy of mixing in the FM state has a minimum at about 5 at.% Cr and changes sign at 6 at.%. The minimum gradually shifts toward Fe as magnetization decreases and the enthalpy becomes positive for $m = 0.92$ (not shown in the figure).

The accuracy of the total energy EMTO-CPA calculations for the Fe-Cr random alloys is confirmed by the supercell full-potential PAW calculations using VASP code: If the local lattice relaxations are ignored, the PAW supercell and EMTO-CPA results are practically the same as can be clearly seen in Fig. 3. One can also see that the local lattice relaxation energy, which is the difference between the total energies of the supercells with and without local lattice relaxations (the form of the supercell should be kept fixed in order to provide the average symmetry of the bcc underlying lattice), is asymmetric and relatively small. We find that a very good fit for this energy is provided by the following expression:

$$E_{\rm rel} = -0.61c(1-c)(1+2.382c), \qquad (3)$$

where $c$ is atomic fraction of Cr and the relaxation energy $E_{\rm rel}$ is in mRy/atom.

The relaxation energy is obtained in the FM state at the theoretical lattice parameters. At the same time, it is clear that it depends on the magnetic state, lattice parameter, and atomic short-range order. Unfortunately, first-principles calculations of such dependencies are too cumbersome. Therefore, in the following, we will neglect them assuming that the relaxation energy is given by Eq. (3), which cannot influence much the final results due to its relatively small value.

In Fig. 3 we also show experimental data for high-temperature enthalpies of formation of Fe-Cr alloys.[55,56] At these temperatures (1200–1500 K) the alloys are in the paramagnetic state, thus it is quite tempting to compare these data with the theoretical DLM results. However, such a comparison should be done cautiously due to the fact that the 0 K DLM calculations take into consideration neither magnetic nor atomic short-range-order effects, which should be present in real alloys. Besides, they are obtained for quite different lattice parameters (theoretical 0 K instead of high temperature), and different types of excitations, for example, vibrational, electronic, and magnetic are also neglected in the DLM 0 K calculations. We will analyze all these effects below, but, first, we will start from a consideration of magnetic excitations, which are obviously one of the strongest and most important in the thermodynamics of Fe alloys.

## IV. THERMODYNAMICS OF MAGNETIC EXCITATIONS IN BCC Fe

### A. Magnetic energy

As has been mentioned above, one of the main problems in the theoretical description of the phase equilibria in Fe alloys is the absence of efficient and accurate first-principles methods for finite temperature thermodynamic properties of itinerant magnets. Nevertheless, the LSDA and GGA are generally believed to be quantitatively accurate for modeling of the energetics of magnetic excitations at high temperatures.

There are several reasons behind such a belief. First of all, the LSDA and GGA accurately reproduce the magnon spectrum and spin-stiffness constant of Fe (see, for instance, Refs. 57–60), which are related to the low-temperature magnetic excitations. Second, the magnetic exchange interactions obtained in the paramagnetic (DLM) state in the LSDA calculations accurately reproduce the Curie temperature in bcc Fe.[61,62] At the same time, there is an unresolved issue with the magnetic energy of bcc Fe.[16]

In Table I we show the magnetic energy defined as the energy difference between the ferromagnetic and paramagnetic (DLM) states. Theoretical calculations have been done at the fixed lattice constant 2.865 Å using different approximations for the exchange-correlation energy (LDA-GGA) and different electronic structure methods (EMTO and PAW). We have also used two different approaches. Namely, the magnetic energy has been obtained in the direct total energy calculations of the

TABLE I. Magnetic energy (in mRy), determined as the difference of the total energies of the ferromagnetic and paramagnetic (DLM) states at a fixed lattice constant (2.865 Å).

| Method | LDA | GGA |
|---|---|---|
| | Total energy calculations | |
| EMTO-FCD | 13.5 | 15.2 |
| PAW | 13.1 | 14.9 |
| | Magnetic exchange interactions | |
| FM | 8.3 | 8.7 |
| DLM | 14.5 | 16.3 |

bcc Fe in the FM and DLM states as well as from the magnetic exchange interaction parameters.

The results from the total energy calculations are shown in the upper part of Table I. The PAW calculations have been performed by the VASP code for a 64-atom supercell, where, in the case of the DLM spin configuration, Fe atoms with spin-up and spin-down local magnetic moments have been distributed in the unit cell in such a way that the pair correlation functions for the first eight coordination shells corresponded to that in a completely random alloy. Note that such supercell calculations yield only an approximate description of the DLM magnetic configuration if it is not a Heisenberg system since fluctuating local environments of different sites make it extremely difficult to provide the absence of the global magnetic moment.

In particular, in our case, the total magnetic moment of the 64-atom supercell in the DLM configuration was about 0.8 $\mu_B$. Although it is an acceptable magnitude for such a large supercell, it can be the reason for a slight underestimate of the magnetic energy. Nevertheless, the agreement between all the results is very good, especially considering the large effect produced by the approximations for the exchange-correlation energy (LDA vs GGA).

At the bottom of Table I we also present the magnetic energy obtained from the magnetic exchange interaction parameters of the Heisenberg Hamiltonian:

$$H = -\sum_{p} \sum_{i,j \in p} J_p \mathbf{e}_i \mathbf{e}_j, \tag{4}$$

where $J_p$ are the magnetic exchange interaction parameters for a given coordination shell $p$ and $\mathbf{e}_i$ is the direction of the spin at site $i$. In this case the magnetic energy is equal to $J_0 = \sum_p z_p J_p$, where $z_p$ is the coordination number of the $p$th coordination shell. The exchange interaction parameters have been calculated using a magnetic force theorem[57] in the FM and DLM states. The origin of the large difference between the FM and DLM magnetic exchange interaction parameters, their consistency with the energetics of magnetic excitations in the FM and DLM states, as well as their relation to the Curie temperature are discussed in Ref. 61.

The important point here is that bcc Fe is not a Heisenberg magnet since its exchange interaction parameters are dependent on the magnetic state. Nevertheless, these exchange interaction parameters provide a quite accurate description of the magnetic configuration close to the one in which they are determined, that is, they are well defined energetic parameters in the corresponding region of the magnetic phase space.[61]

One can also see that the magnetic energy obtained in the direct total energy calculations is in between the results from the magnetic exchange interaction parameters in the FM and DLM states. In other words, the two different methods yield approximately the same result for the magnetic energy which is roughly about 13–14 mRy in the LSDA and about 15 mRy in the GGA.

The problem here, as has been already mentioned by Korzhavyi *et al.*,[16] is the fact that *ab initio* (LSDA/GGA) magnetic energy is about twice as large as the existing experimental estimate of about 7 mRy, which is deduced from the heat capacity data for Fe by subtracting model electronic and vibrational contributions.[12] The latter is used in the CALPHAD modeling.[3] Since the magnetic energy is very large (can be, for instance, compared with the mixing enthalpies presented in Fig. 3), it is extremely important to understand where this difference can originate from.

### B. Paramagnetic state

Unfortunately it is very hard to solve the issue of the accuracy of the LSDA/GGA-based *ab initio* methods for the magnetic energy. In general, it requires the comparison with the first-principles methods, which treat accurately the finite-temperature magnetic excitations. The existing dynamical-mean-field theory (DMFT) calculations still do not satisfy the criteria of being parameter-free, and they produce quite a large error for the Curie temperature (about 1900 K in Ref. 63 and 1600 K in Ref. 64), the reason for which is not known. Therefore, we assume here that the main problem is not related to the errors of the LSDA and GGA used in our work.

As a matter of fact, there is an indication that the experimentally assessed magnetic energy is quite largely underestimated. In Fig. 4 we show the magnetic heat capacity above the Curie temperature obtained in the classical Heisenberg Monte Carlo (MC) simulations with the LSDA magnetic exchange interaction parameters[61] and the fit of the accepted assessment of the experimental data in the CALPHAD method.[3] At first sight the difference between the theoretical heat capacity and

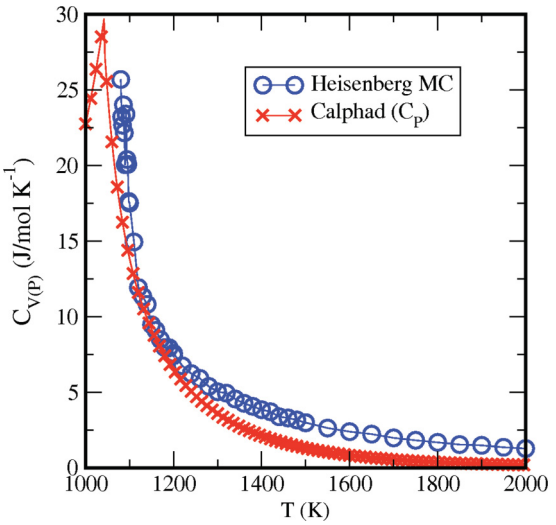


FIG. 4. (Color online) Magnetic heat capacity from classical Heisenberg MC calculations and adopted in the CALPHAD method.[3]

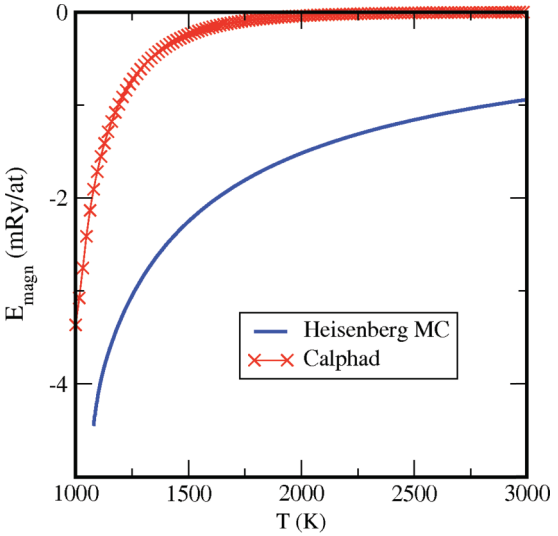


FIG. 5. (Color online) Magnetic energy relative to that in the infinite temperature limit from classical Heisenberg MC calculations and "experimental" data adopted in the CALPHAD method.

the data used in the CALPHAD method is not large. However, they produce quite different magnetic energy relative to the "ideal" paramagnetic state as can be clearly seen in Fig. 5.

According to the recent investigation by Körmann *et al.*,[65] the heat capacity and entropy in the classical MC simulations are very close to those in the quantum MC above the magnetic transition temperature. Thus, the presented above classical MC results can be considered as an accurate representation of the Heisenberg model, especially in the high-temperature limit, where there exists a significant difference between the "experimental" data adopted in the CALPHAD method[3] and MC results. At the same time it is likely that the Heisenberg model yields the lowest boundary for the heat capacity in the case of bcc Fe since there should be an additional contribution to the specific heat in bcc Fe due to the longitudinal spin fluctuations.[62]

In fact, the experimental data for the heat capacity in the paramagnetic state are largely scattered,[66] which apparently reflects the problems with its experimental determination at high temperatures. This means that the magnetic energy accepted in the latest CALPHAD evaluation,[3] which obtained from the assessment of the heat capacity data, can be indeed underestimated.

### C. Low-temperature ferromagnetic state: Noninteracting magnons

Magnetic excitations at low temperatures are magnons and their contribution to the thermodynamic properties can be obtained either from the corresponding spin-spiral calculations or much easier from the magnetic exchange interaction parameters of the Heisenberg Hamiltonian determined in the FM state. Such calculations for Fe, Co, and Ni have been, for instance, previously done by Halilov *et al.*[58,67] on the basis of *ab initio* magnetic exchange interactions. Here we use the same magnon adiabatic approach neglecting magnon-magnon interactions.

In this case, the magnon occupation numbers $n_{\mathbf{q}}$ for wave-vector $\mathbf{q}$ at temperature $T$ are given by the Plank distribution function:

$$n_{\mathbf{q}} = \frac{1}{\exp(E_{\mathbf{q}}/k_B T) - 1}, \tag{5}$$

where

$$E_{\mathbf{q}} = \frac{4}{M}[J_{\mathbf{q}} - J_0] \tag{6}$$

is the magnon spectrum determined from the Fourier transform of magnetic exchange interaction parameters $J_p$ defined in Eq. (4), $J_{\mathbf{q}} = \sum_p \sum_{i,j\in p} J_p \exp(-i\mathbf{q}\mathbf{R}_{ij})$ and $J_0 \equiv J_{\mathbf{q}=0}$. Here $M$ is the magnetic moment of Fe in $\mu_B$.

Spin-wave amplitudes $\theta_{\mathbf{q}}$, which are proportional to the number of the corresponding excited magnons $n_{\mathbf{q}}$, as $\theta_{\mathbf{q}}^2 = 2n_{\mathbf{q}}$,[67] are actually the azimuth angles of the corresponding spin waves relative to the axis of the global magnetization. Therefore, the resulting reduced magnetization $m$ is

$$m = \sum_{\mathbf{q}} \cos\theta_{\mathbf{q}}. \tag{7}$$

The magnetic exchange interaction parameters up to the 150th coordination shell have been calculated by the EMTO method using the magnetic force theorem[57] in the FM state for the lattice parameter of 2.865 Å. In Fig. 6 we show the magnon spectrum in the $\Gamma$-$P$ direction of the bcc Brillouin zone calculated from the magnetic exchange interaction parameters as well as from the EMTO total-energy spin-spiral calculations with a small azimuth angle of $0.05\pi$. As one can see, they agree quite well with each other and with the experimental data.[68] As has been already mentioned, good agreement with the existing experimental data has been obtained in a number of the previous DFT calculations.

In Fig. 7 we show the calculated reduced magnetization, where we compare it with the experimental data[68] and classical Heisenberg Monte Carlo results. It is, of course, very similar to the results obtained by Halilov *et al.*.[58,67] One can see that

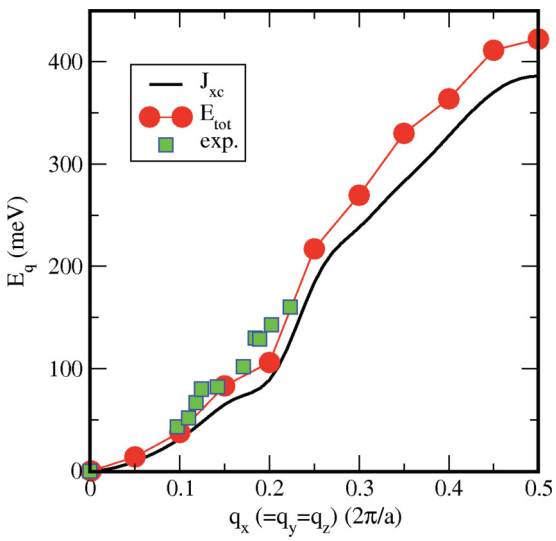


FIG. 6. (Color online) The magnon spectrum in the $\Gamma$-$P$ direction of the bcc Brillouin zone obtained from magnetic exchange interactions in the FM state (solid line), total energy spin-spiral calculations azimuth angle is $0.05\pi$ (filled circles), and experimental data (squares).[68]

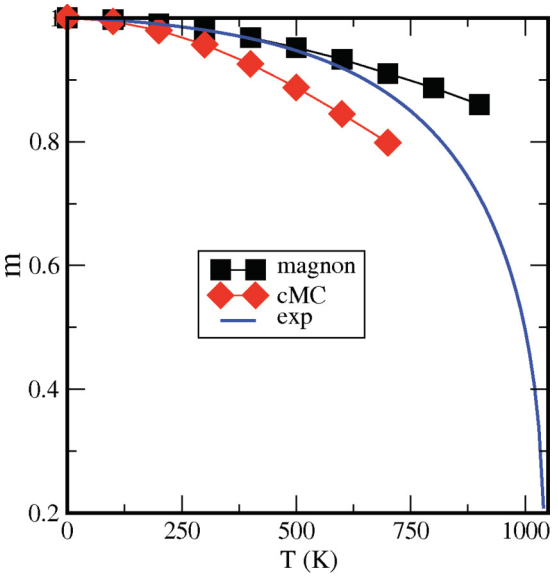


FIG. 7. (Color online) Reduced magnetization: Noninteracting spin-wave calculations (squares), classical Monte Carlo (cMC) results (diamonds), and experimental data (solid line).

the spin-wave approach reproduces accurately the experimental reduced magnetization up to about 400–500 K. Above this temperature the magnon-magnon interactions become important together with other types of magnetic excitations. The latter can be also clearly seen in Fig. 8 where we compare the magnon heat capacity, obtained from the energy of the noninteracting spin-wave excitations, with that used in the CALPHAD method.[69] The increase of the magnon heat capacity is apparently too weak above 400 K.

### D. Finite temperature ferromagnetic state: PDLM model

It is clear that a simple model of noninteracting magnons breaks down at quite low temperatures, where the reduce magnetization is still very high. At the same time, accurate

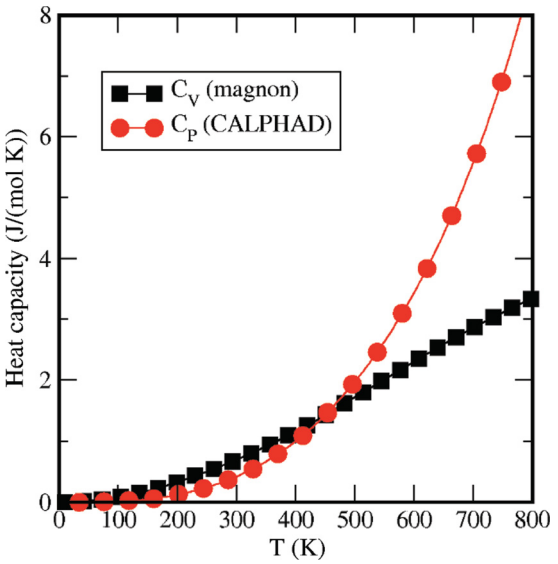


FIG. 8. (Color online) Heat capacity: Noninteracting spin-wave calculations and CALPHAD data.

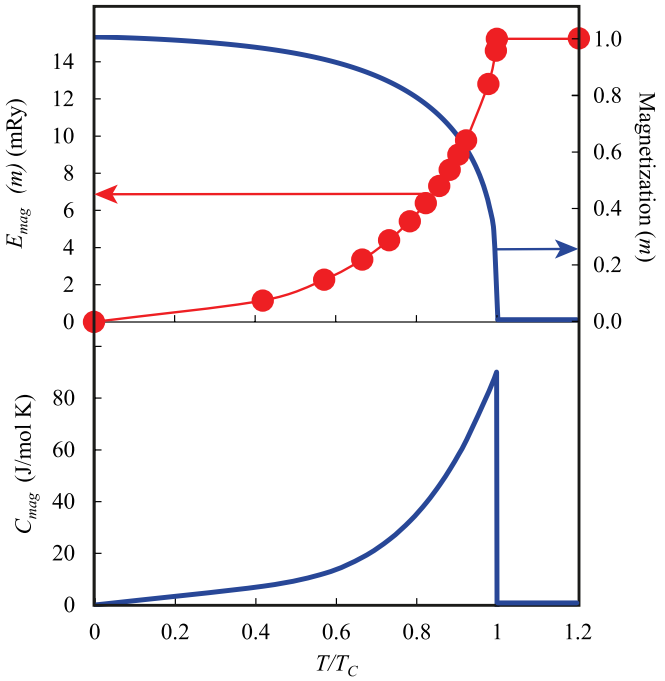


FIG. 9. (Color online) The magnetic energy of bcc Fe as a function of the reduced temperature (top panel), calculated for particular magnetization $m$, which is determined from temperature $T$, using parametrization (8) from Ref. 71 (bottom panel).

first-principles calculations of the reduced magnetization in the whole temperature range are extremely complicated. Therefore, we employ the existing experimental data, similar to the work by Körmann *et al.*,[65] where it has been used in the statistical modeling. The temperature dependence of magnetization for pure iron was experimentally obtained by Crangle and Goodman[70] and fitted to a simple analytical expression by Kuzmin:[71]

$$m(T) = [1 - 0.35\tau^{3/2} - (1 - 0.35)\tau^4]^{1/3}, \qquad (8)$$

where $\tau = T/T_C$ is the reduced temperature and $T_C$ is the Curie temperature, which is presented in Fig. 7.

In the first-principles calculations of the FM state with a reduced magnetization $m$, we use the PDLM model described above, where the magnetization determines the relative concentration of spin-up and spin-down Fe atoms. In Fig. 9 we show the PDLM magnetic energy of bcc Fe (relative to the energy of the fully ordered FM configuration), as a function of the reduced temperature obtained in the EMTO PDLM calculations at the *experimental* lattice constants for the corresponding temperatures.[72]

The magnetic energy follows closely the change of the magnetization. When the paramagnetic (DLM) state is reached, the magnetic energy is almost constant (there is little temperature dependence due to the temperature-dependent lattice constant). Thus, the heat capacity at constant pressure $P$, determined as

$$C_P^{\mathrm{PDLM}} = \left(\frac{\partial E_{\mathrm{tot}}^{\mathrm{PDLM}}}{\partial T}\right)_P, \qquad (9)$$

will have the temperature dependence, shown in the lower panel of Fig. 9. As one can see, such a simple single-site

mean-field model for the magnetic energy results in the zero heat capacity above the Curie temperature, in the DLM state, representing the ideal paramagnetic state, where the magnetic short-range-order (SRO) effects are neglected. At the same time, as has been shown above, the magnetic energy associated with the magnetic short-range order is large, especially close to the magnetic transition. Therefore, in order to have accurate description of magnetic energetics, the *whole* PDLM model should be corrected.

### E. Magnetic short-range-order correction

The only way to take the magnetic short-range-order effects into consideration in the present DFT calculations is to add them *ad hoc* using, for instance, the results of the classical Heisenberg Monte Carlo simulations above the Curie temperature.[61,73] The starting point for modeling here can be the heat capacity, which can be divided in two temperature intervals, below and above the Curie temperature:

$$C_P^{\mathrm{mod}}(T) = \begin{cases} C_P^{\mathrm{FM}}(T) & \text{if } T < T_C; \\ C_P^{\mathrm{PM}}(T) & \text{if } T > T_C, \end{cases} \tag{10}$$

where $C_P^{\mathrm{FM(PM)}}$ is the heat capacity of the FM (PM) state at constant pressure.

A simple and convenient choice for $C_P^{\mathrm{FM}}$ is a parametrization used by Inden:[74]

$$C_P^{\mathrm{FM}}(T) = K \ln \frac{1+\tau^3}{1-\tau^3}, \tag{11}$$

where $K$ is the fitting constant and $\tau = T/T_C$ is the reduced temperature. The magnetic heat capacity above the Curie temperature in the paramagnetic state $C_P^{\mathrm{PM}}$ has been chosen to be equal to that obtained in the classical Heisenberg Monte Carlo simulations. It is substantially greater than that adopted in the CALPHAD by Xiong *et al.*,[3] which practically vanishes above 2000 K. As has been mentioned above, the theoretical value of the heat capacity can be even higher in the paramagnetic state due to the presence of the longitudinal spin fluctuations.

To obtain $C_P^{\mathrm{mod}}$ consistent with the fist-principles results, one should impose the following normalization condition:

$$\int_0^\infty C_P^{\mathrm{mod}}(T)dT = E_{\mathrm{tot}}^{\mathrm{DLM}} - E_{\mathrm{tot}}^{\mathrm{FM}}, \tag{12}$$

where $E_{\mathrm{tot}}^{\mathrm{DLM(FM)}}$ is the total energy of Fe in the DLM(FM) state.

In Fig. 10 we show the magnetic heat capacity determined in this way together with the CALPHAD adopted data, Monte Carlo results, and heat capacity from the EMTO total energy calculations. The shaded area is the difference between the model and PDLM heat capacity, obtained in the EMTO total energy calculations. It determines the additional contribution to the total energy, which should be added to the EMTO total energy to make a consistent description of the thermodynamic properties. So, the model magnetic energy, which takes the magnetic SRO effects above the Curie temperature into consideration $[E_{\mathrm{mag}}^{\mathrm{mod}}(T)]$ is

$$E_{\mathrm{mag}}^{\mathrm{mod}}(T) = E_{\mathrm{mag}}(T) + \int_0^T \left[C_P^{\mathrm{mod}}(T) - C_P^{\mathrm{PDLM}}(T)\right]dT, \tag{13}$$

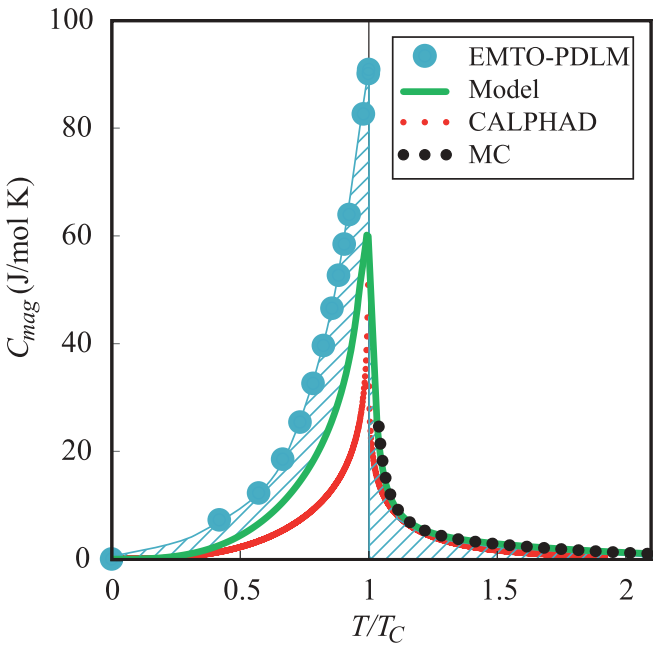


FIG. 10. (Color online) "Magnetic" heat capacity of iron. The EMTO-PDLM total energy results (large circles) assume that the DLM state is achieved at the Curie temperature (no magnetic SRO); model results include renormalization due to magnetic SRO effects above $T_C$ obtained within the proposed magnetic model; CALPHAD data (broken line) and Heisenberg MC results (dots). The shaded areas represent the corrections to the EMTO-CPA total energies due to the magnetic SRO.

where $E_{\mathrm{mag}}(T)$ is the magnetic energy determined in the PDLM calculations.

It is shown in Fig. 11 where it is compared with the PDLM results. One can clearly see quite a strong reduction of the model magnetic energy in the paramagnetic state close to the Curie temperature compared to that in the PDLM calculations. The model magnetic energy at 1500 K is 9 mRy, which is much lower than without magnetic energy correction of about 16 mRy. Such a strong reduction of the magnetic energy due to the magnetic SRO reconciles to a large extent *ab initio* theory and evaluations based on the experimental heat capacity. In fact, the agreement would be better if the LSDA is used instead of the GGA in the total energy calculations. The correction also strongly affects the magnetic free-energy in the PDLM, as can be seen in the bottom panel of Fig. 11. The entropy contribution in this case has been determined from the heat capacity as

$$\Delta S(T) = \int_0^T \frac{C_P}{T} dT. \tag{14}$$

## V. ATOMIC ALLOY CONFIGURATION OF Fe-Cr ALLOYS

In order to calculate thermodynamic properties of Fe-Cr alloys, one should first determine the proper atomic configuration as a function of concentration and temperature or choose the corresponding model. There exist several experimental studies of the atomic SRO in Fe-Cr alloys at different alloy

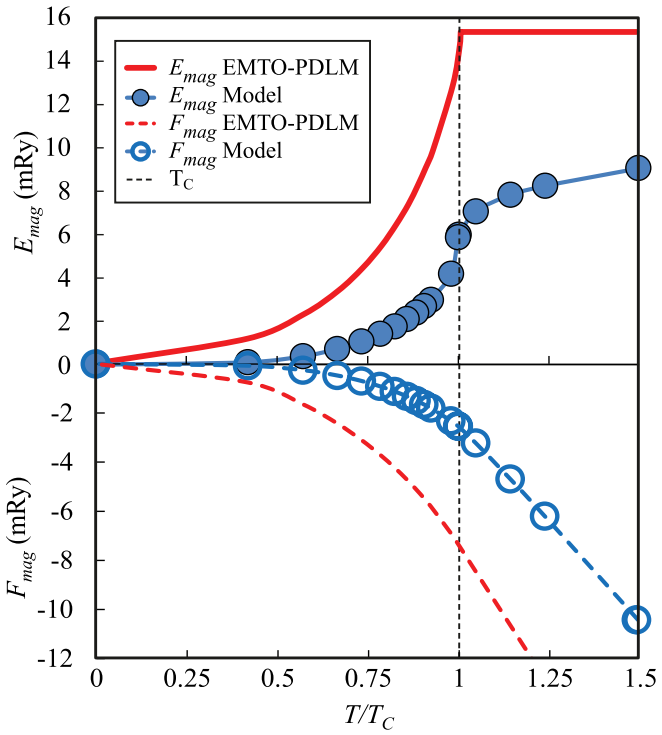


FIG. 11. (Color online) Magnetic energy (top panel) and magnetic free-energy (bottom panel) of Fe obtained with the correction for the magnetic SRO in the paramagnetic state. It is compared with that obtained in the DPLM calculations.

compositions and temperatures.[8,19,20,75] The experimental data indicate that it is relatively small. Nevertheless, its effect on the thermodynamic properties of Fe-Cr alloys remain unclear. In this section we use first-principles methods in order to calculate such an effect.

Such calculations are also important as a test of the applied theoretical methods and models. In this particular case, it concerns the validity of the (P)DLM approach for the quantitatively accurate description of chemical interactions in the corresponding magnetic state. In this paper we will consider equiatomic alloy at 1100 K in the paramagnetic state and Fe-rich alloys at 700 K in the ferromagnetic state with reduced magnetization.

The configurational Hamiltonian has been defined as

$$H_{\text{conf}} = \frac{1}{2}\sum_{p} V_p^{(2)} \sum_{i,j\subset p} \delta c_i \delta c_j + \cdots, \qquad (15)$$

where $V_p^{(2)}$ are the pair effective interactions for the corresponding coordination shell of the bcc lattice denoted by $p$. The $\delta c_i$ are the concentration fluctuations at sites $i$; $\delta c_i = c_i - c_{\text{Cr}}$, where $c_i$ is the occupation number at site $i$, taking on values 1 or 0 if the site $i$ is occupied by a Cr or Fe atom, respectively.

The effective interactions in the PDLM state have been calculated using the corresponding average over a magnetic state by the screened generalized perturbation method (SGPM),[17,31,61] which is a generalization of the GPM,[76,77] including screened Coulomb interactions defined within DFT. The SGPM calculations have been done using EMTO-CPA code as described in Ref. 17. The screened Coulomb interactions have been obtained in the LSGF supercell calculations.[31]

In fact, the SGPM yields only the so-called chemical contribution to the effective cluster interaction, while there is, for instance, a vibrational contribution neglected here. Another contribution is expected to be from the strain-induced interactions, however, they should be relatively small since the concentration dependence of the lattice constant in the high-temperature paramagnetic state is quite weak (see Fig. 1).

### A. Atomic SRO of Fe-rich FeCr alloys in the FM state

Here we would like to demonstrate that the PDLM model provides a description consistent with experiment of the chemical interactions in the Fe-rich Fe-Cr alloys in the ferromagnetic state at elevated temperatures, when magnetization is reduced. In fact, such calculations have been already done in Ref. 17. However, the alloy composition has been fixed to $Fe_{0.9}Cr_{0.1}$. Recently, Mirebeau and Parette,[20] using neutron diffuse scattering, have studied the atomic SRO in the concentration range of $0 < c_{\text{Cr}} < 15$ at.% at 700 K, which is in the ferromagnetic state.

This gives us an opportunity to check the concentration dependence of the effective chemical interactions. For that purpose we have calculated the effective pair interactions in the concentration interval of $0 < c_{\text{Cr}} < 25$ at.% using the SGPM method.[17] The calculations have been done for a fixed lattice constant of 2.88 Å and the reduced magnetization of 0.85, which are close to the corresponding experimental data for pure Fe at 700 K. Although both the lattice parameter and magnetization depend on concentration, such a dependence is not known. At the same time, the reduced magnetization cannot deviate strongly from this magnitude since the Curie temperature changes little within the concentration range up to 20 at.% Cr.

In Fig. 12 we show our results and experimental data from Ref. 20 for the weighted average of the first two effective pair interactions $\langle V_{12}\rangle = (8V_1 + 6V_2)/14$ as a function of Cr concentration. The agreement between theory and experiment is very good (let us note that the theoretical results presented in Ref. 20 are for the 0 K FM state). Thus, the used approximations and models in the *ab initio* calculations are indeed quantitatively accurate for the description of the chemical interactions in Fe-Cr alloys.

Nevertheless, one should bear in mind that the effective pair interactions presented in Fig. 12 and in Ref. 17 should be considered as *median* since the effective pair interactions in the Fe-rich Fe-Cr alloys are dependent on the local atomic environment in the FM state.[16] This also means that the Ising Hamiltonian in the form of Eq. (15) is not valid for the accurate description of the configurational thermodynamics. However, a detail consideration of these effects is beyond the aim of this paper.

### B. Atomic SRO of equiatomic FeCr alloy in the PM state

The atomic SRO parameters in bcc $Fe_{0.53}Cr_{0.47}$ alloy were determined in the anomalous x-ray-scattering study by

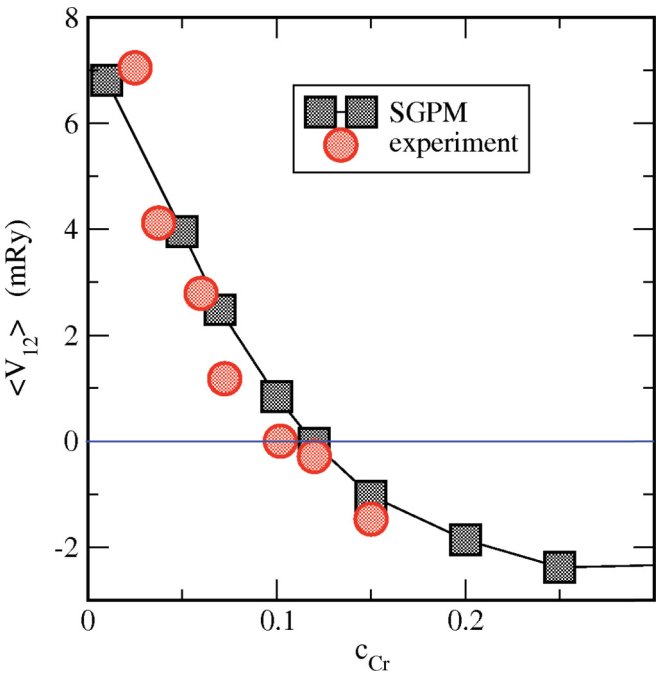


FIG. 12. (Color online) Average effective pair interaction at the first two coordination shells (squares) obtained in the PDLM calculations for reduced magnetization 0.85, which corresponds to 700 K. Experimental from Ref. 20.

Reinhard *et al.*[75] and theoretically investigated by Turchi *et al.*,[8] who determined the effective pair interactions by the GPM within Korringa-Kohn-Rostoker (KKR)-CPA calculations, which were done for the nonmagnetic (NM) state and without the contribution from the screened Coulomb interactions.

Here we use the SGPM, which as has been mentioned above, to contain an additional electrostatic contribution due to screened Coulomb interactions.[31,61] Calculations have been done for a random equiatomic alloy within the LSDA at the experimental lattice constant 2.695 Å at 1100 K, which was the annealing temperature in the experimental study.

In Table II we compare our results for the effective pair interactions obtained in the DLM and NM states with the NM-GPM-KKR results by Turchi *et al.*[8] and the experimental data from the inverse Monte Carlo simulations.[75] The DLM SGPM-EMTO effective pair interactions (first column) are the one which should be compared with the experimental data, and one can see that they are in reasonably good agreement.

One can also notice that the first two NM GPM-KKR interactions by Turchi *et al.*[8] are also in very good agreement with the experimental data. However, this agreement is accidental, and, as we show here, the nonmagnetic description of the paramagnetic state results in the large error for the effective chemical interactions. The origin of the good agreement in this particular case is the compensation of errors: The error due to the nonmagnetic description is, in fact, compensated by the error due to unaccounted screened Coulomb interactions in the GPM-KKR calculations.[8]

To clarify this point we have also performed NM SGPM calculations of the effective interactions, which are shown in the third column of Table II. As one can see, they are

TABLE II. Effective pair interactions $V_p^{(2)}$ ($p = \{lmn\}$) obtained in the present SGPM-EMTO calculations in the DLM and NM states, previous NM GPM-KKR calculations[8] and deduced from the experimental data.[75]

| | $V_{lmn}^{\mathrm{ch}}$ (mRy) | | | | |
|---|---|---|---|---|---|
| | SGPM-EMTO | | | GPM-KKR, Ref. 8 | |
| *lmn* | DLM | NM | NM (one-el.) | NM (one-el.) | Expt. |
| 111 | − 3.614 | − 0.322 | − 3.731 | − 4.34 | − 4.00 |
| 200 | 0.837 | 1.857 | 0.646 | 0.62 | 0.53 |
| 220 | − 0.157 | 0.131 | 0.339 | 0.70 | 0.09 |
| 311 | 0.017 | 0.434 | 0.470 | 0.46 | − 0.06 |
| 222 | − 0.156 | − 0.743 | − 0.726 | − 0.88 | 0.04 |
| 400 | 0.149 | 0.264 | 0.264 | 0.29 | 0.28 |
| 331 | 0.071 | 0.101 | 0.063 | 0.06 | 0.09 |
| 420 | 0.006 | − 0.002 | − 0.011 | | − 0.03 |
| 422 | 0.021 | 0.032 | 0.032 | | 0.00 |
| 511 | 0.004 | − 0.018 | − 0.018 | | − 0.04 |
| 333 | − 0.024 | 0.177 | 0.177 | | − 0.01 |

quite different from the interactions in the paramagnetic DLM state. At the same time, they are in reasonable agreement with the NM GPM-KKR calculations for all the coordination shells, but the first three. The large difference at the first three coordination shells is due to the additional electrostatic contribution, which is absent in the GPM-KKR calculations[8] since the one-electron part of the effective interactions in the NM GPM-EMTO (the third column) is indeed in good agreement with that of the NM GPM-KKR calculations.

Since the strongest interactions are well reproduced by the present theory, we can conclude that the DLM and LSDA provides quite accurate description of the chemical bonding in paramagnetic Fe-Cr alloys. At this point, one can wonder about the effect of the magnetic SRO on the atomic SRO and vice versa. They can be indeed coupled, but such a coupling, if it exists, should be very weak in the case of equiatomic Fe-Cr alloys at 1100 K due strongly reduced magnetic SRO: The Curie temperature for that alloy is about 600 K (see the next section) and besides, the Cr atoms should give very little contribution to the transverse spin fluctuations.

Finally, using the SGPM-EMTO interactions, we calculate the free-energy of the atomic SRO as a function of temperature assuming that the interactions are temperature independent. Note that the effect of the atomic SRO is strongest for the equiatomic alloy composition if the pair effective interactions do not depend on the alloy composition.[78]

In Fig. 13 we show the contribution of the atomic SRO to the free-energy of a completely random equiatomic alloy, which has been determined from the SGPM-EMTO interactions listed in Table II in the ring-mean-field calculations.[79] It is relatively small, which makes it possible to disregard the atomic SRO effects in the first-principles thermodynamic modeling, considering only completely random alloys. This will significantly simplify the study, because it is a rather nontrivial task to take into consideration the coupling between the atomic SRO and local magnetic structure, especially in the FM state, although the latter it is very interesting and important, but deserves a separate investigation.

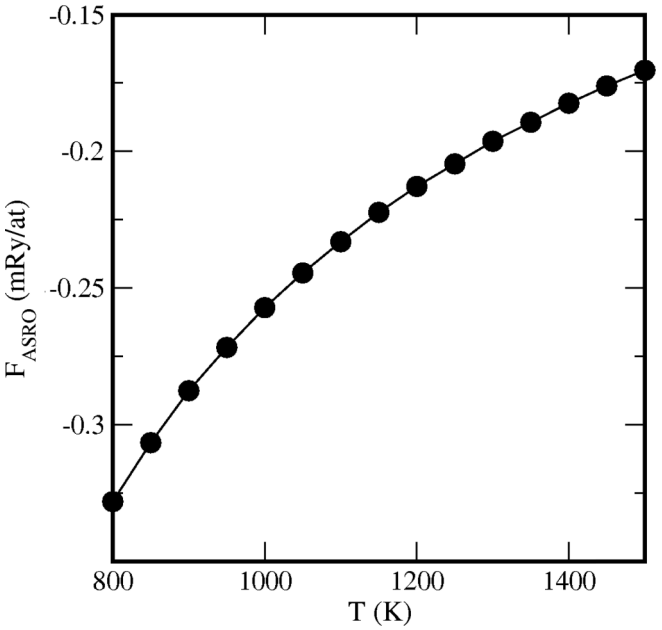


FIG. 13. Free-energy of the atomic SRO, $F_{\mathrm{ASRO}}$ of $Fe_{50}Cr_{50}$, obtained in the ring-mean-field from SGPM effective pair interactions.

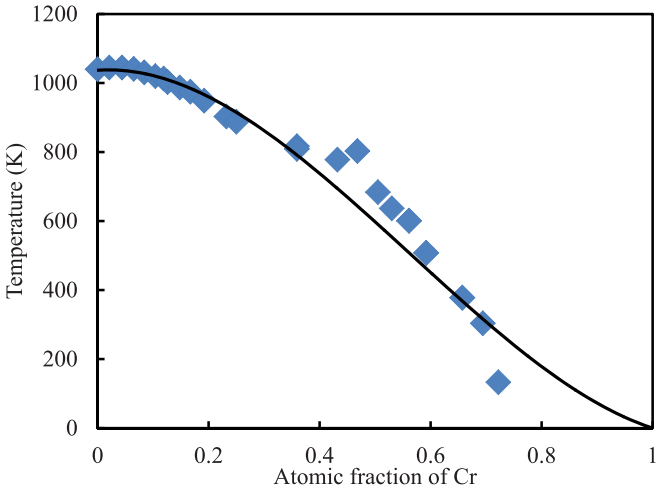


FIG. 14. (Color online) The experimental Curie temperature of Fe-Cr alloys[80] and its polynomial fit used in the work for theoretical modeling.

## VI. THERMODYNAMIC PROPERTIES OF RANDOM ALLOYS

### A. Magnetic model for alloys

It is well known that the Cr-rich Fe-Cr alloys containing less than 20 at.% Fe and pure Cr form different types of spin density wave magnetic structures below the Néel temperature, which has a maximum value of 310 K for pure Cr.[82] Above this temperature these alloys are however in the paramagnetic state, and therefore the low-temperature magnetic structures can be neglected in the phase diagram calculations at elevated temperatures.

At the same time, the zero-temperature consideration is needed as a starting point in order to build a consistent model for the phase equilibria. Thus, we will assume that the zero-temperature magnetic state is ferromagnetic for the whole concentration range. Since the magnetic energy is quite small in the case of Cr-rich alloys anyway,[16] this assumption cannot influence much the results in the paramagnetic state.

In order to build a model for the magnetic energy of alloys, we also need to specify the magnetic state for each alloy composition and temperature. Fortunately there exist experimental data for the Curie temperature, which determines the boundary between paramagnetic and ferromagnetic states. In Fig. 14 we show the experimental data for the Curie temperature in Fe-Cr alloys.[80] To simplify theoretical consideration we use a polynomial fit, which is also shown in the figure. Since there are no experimental data for the reduced magnetization in Fe-Cr alloys, we will assume that it is the same function of temperature as in the case of pure Fe, that is, it is determined by Eq. (8). Thus, these two analytical fits specify the magnetic state at all the points in the concentration-temperature coordinates.

The magnetic SRO energy is quite large close to the Curie temperature (see above), and therefore it should be taken into consideration in the case of alloys too. Although the corresponding classical Heisenberg Monte Carlo simulations are possible, we have chosen the same analytical form for the magnetic heat capacity as in the case of pure Fe. This model is quite approximate for alloys close to equiatomic composition.[74] Nevertheless, as will be shown below, this region does not actually play a significant role in the phase diagram calculations below the Curie temperature. At the same time, the model is reasonable for the Fe-rich composition, which is important.

Thus, we assume that the magnetic heat capacity in the case of Fe-Cr alloys has a similar shape as in the case of pure Fe, that is, it is given by Eqs. (10) and (11). However, it is rescaled by a factor, which takes into consideration the change of the whole magnetic energy (per atom) of an alloy (see Fig. 14 in Ref. 16). Let us mention that such a rescaling of the magnetic heat capacity of the alloys is similar to the "parallel shift method."[81,83,84] The difference between this method and ours is that instead of multiplying the magnetic heat capacity of iron by the iron (or chromium) content, we normalize the magnetic heat capacity by the magnetic energy of the alloy obtained in the first-principles calculations.

### B. Free-energy of lattice vibrations: The average force constants model

First-principles calculations of the phonon spectrum in random alloys require the use of quite nontrivial and time-consuming techniques.[85–88] It is an especially difficult task in magnetic systems at high temperatures. Therefore, in this work, we adopt a simplified approach, which serves one purpose: To provide a reasonable model for the vibrational contribution to the free-energy of alloys in the thermodynamic modeling. Recently, Alam *et al.*[88] formulated and used the augmented space formalism for the calculations of the phonon spectrum and phonon entropy in Fe-Cr alloys, however, it is quite heavy in the implementation. Therefore, we propose a simplified average force constants model (AFCM), which should be quite accurate in the dilute limit.

Within the AFCM, the force constants of a binary alloy are given by the average "medium" force constant matrix $\tilde{\Phi}_{\alpha\beta}(\mathbf{R})$, which relates the force $f_\alpha$ exerted on a medium atom in the $\alpha$ direction due to the displacement $u_\beta$ of the atom in position $\mathbf{R}$ relative to the first one in the $\beta$ direction ($\alpha$ and $\beta$ are the indices of the three Cartesian coordinates). Assuming that the force constants do not depend on the local environment, which is the case of the dilute limit, the average force constant matrix is

$$\tilde{\Phi}_{\alpha\beta}(\mathbf{R}) = c^2\Phi^{\mathrm{CrCr}}_{\alpha\beta}(\mathbf{R}) + 2c(1-c)\Phi^{\mathrm{FeCr}}_{\alpha\beta}(\mathbf{R}) + (1-c)^2\Phi^{\mathrm{FeFe}}_{\alpha\beta}(\mathbf{R}), \quad (16)$$

where $\Phi^{\mathrm{XY}}_{\alpha\beta}(\mathbf{R}) = f^{\mathrm{X}}_\alpha/u^{\mathrm{Y}}_\beta$ is the force constant matrix for two sites separated by $\mathbf{R}$ and occupied by X and Y atoms, and $c$ is the atomic fraction of Cr.

The force constants have been calculated by the PAW method using the VASP code (the details of the calculations are given above) for dilute limit of Cr in Fe and vice versa, Fe in Cr. In the first case, the calculations have been done at the Fe room temperature lattice constant in the FM state. While the Fe-Fe and Fe-Cr force constants have been determined up to the 13th coordination shell, Cr-Cr force constants have been determined only for the first two coordination shells. Nondiagonal Cr-Cr force constants have been obtained by using the proper average over all the possible displacement of the central Cr atom. The calculations of the force constants in the dilute limit of Fe in Cr have been done in a similar fashion, but at the room-temperature lattice spacing of Cr.

The phonon spectrum has then been determined as for a monoatomic solid using the average atomic mass $\tilde{M} = cM_{\mathrm{Cr}} + (1-c)M_{\mathrm{Fe}}$, where $M_{\mathrm{Cr}}$ and $M_{\mathrm{Fe}}$ are the atomic masses of Fe and Cr. The calculations of vibrational spectra, the phonon free-energy, and entropy in the harmonic approximation have been done by program PHON[43,44] in Fe-rich and Cr-rich alloys using the corresponding force constant matrix.

In Fig. 15 we show the phonon entropy at 300 K obtained within the model presented above, experimental data by Lucas *et al.*[90] and Fultz *et al.*[91] at the same temperature, and the recent first-principles results obtained within the augmented space formalism by Alam *et al.*.[88] As one can see, our model yields quite an accurate description of the phonon entropy. Therefore, in order to use the model in the whole concentration range, we extrapolate the low concentration data for the phonon free-energy on both Fe-rich and Cr-rich sides to the whole range of concentration by third order polynomial. Such an extrapolation for the entropy is shown in Fig. 15 by a solid line.

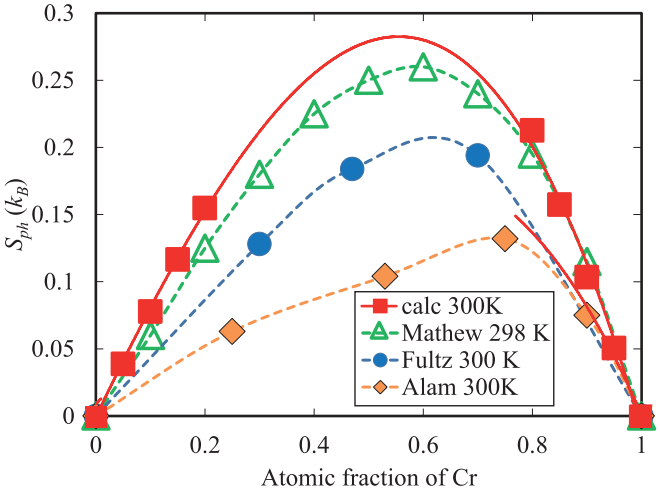


FIG. 15. (Color online) Phonon entropy of Fe-Cr alloys at 300 K. The results of the model are shown by squares, the experimental data by triangles[90] and circles,[91] and augmented spaced formalism results[88] by diamonds.

## VII. PHASE DIAGRAM CALCULATIONS

The Gibbs free-energy of mixing of random alloys Fe-Cr alloys $\Delta G(c,T)$ has been determined as a function of concentration $c \equiv c_{\mathrm{Cr}}$ and temperature $T$:

$$\Delta G(c,T) = \Delta H(c,T) + \Delta G_{\mathrm{ph}}(c,T) + \Delta G_{\mathrm{el}}(c,T) + T\Delta S_{\mathrm{mag}}(c,T) - T\Delta S_{\mathrm{conf}}(c) + E_{\mathrm{rel}}(c). \quad (17)$$

Here $\Delta H(c,T)$ is the electronic and magnetic part of the enthalpy of formation of random $\mathrm{Fe}_{1-c}\mathrm{Cr}_c$ random alloys determined in the total energy (P)DLM calculations and containing the corresponding magnetic energy correction. The total energy calculations have been done for the experimental lattice constants if they were known, otherwise the extrapolated values have been used. Alternatively, the Debye-Grüneisen model[92] could be used. However, it is too cumbersome to take into consideration the magnetic free-energy for every temperature and concentration. Besides, it is not accurate. $E_{\mathrm{rel}}$ is the relaxation energy determined by Eq. (3), which we assumed to be temperature independent.

The phonon contribution $\Delta G_{\mathrm{ph}}(c,T)$ is

$$\Delta G_{\mathrm{ph}}(c,T) = G^{\mathrm{alloy}}_{\mathrm{ph}}(c) - cG^{\mathrm{Cr}}_{\mathrm{ph}} - (1-c)G^{\mathrm{Fe}}_{\mathrm{ph}}, \quad (18)$$

where the phonon free-energy of alloy $G^{\mathrm{alloy}}_{\mathrm{ph}}(c)$ and pure Fe and Cr $G^{\mathrm{Fe}}_{\mathrm{ph}}$ and $G^{\mathrm{Cr}}_{\mathrm{ph}}$ has been obtained as described in Sec. VI B. The force constants have been calculated at the room temperature lattice constant of Fe in the FM state for the Fe-rich part and at the room temperature lattice constant of Cr in the NM state for the Cr-rich part. The temperature dependence of the force constants has been ignored.

The contribution from the thermal one-electron excitations is

$$\Delta G_{\mathrm{el}}(c,T) = G^{\mathrm{alloy}}_{\mathrm{el}}(c,T) - cG^{\mathrm{Cr}}_{\mathrm{el}} - (1-c)G^{\mathrm{Fe}}_{\mathrm{el}}, \quad (19)$$

where $G_{\mathrm{el}}$ is the free-energy correction to the total energy obtained in the direct first-principles calculations, and it is given by[89]

$$G_{\mathrm{el}} = -\frac{\pi^2}{3}N(E_F)k_B^2T^2. \quad (20)$$

Here $N(E_F)$ is the density of states at the Fermi level $E_F$ obtained for the temperature and concentration-dependent lattice constants. The direct calculations of the free-energy correction confirmed the high accuracy of this formula for Fe-Cr alloys.

The magnetic mixing entropy contribution $\Delta S_{\mathrm{mag}}(c,T)$ has been determined from the model heat capacity using Eq. (14). As has been already mentioned, it also includes contributions

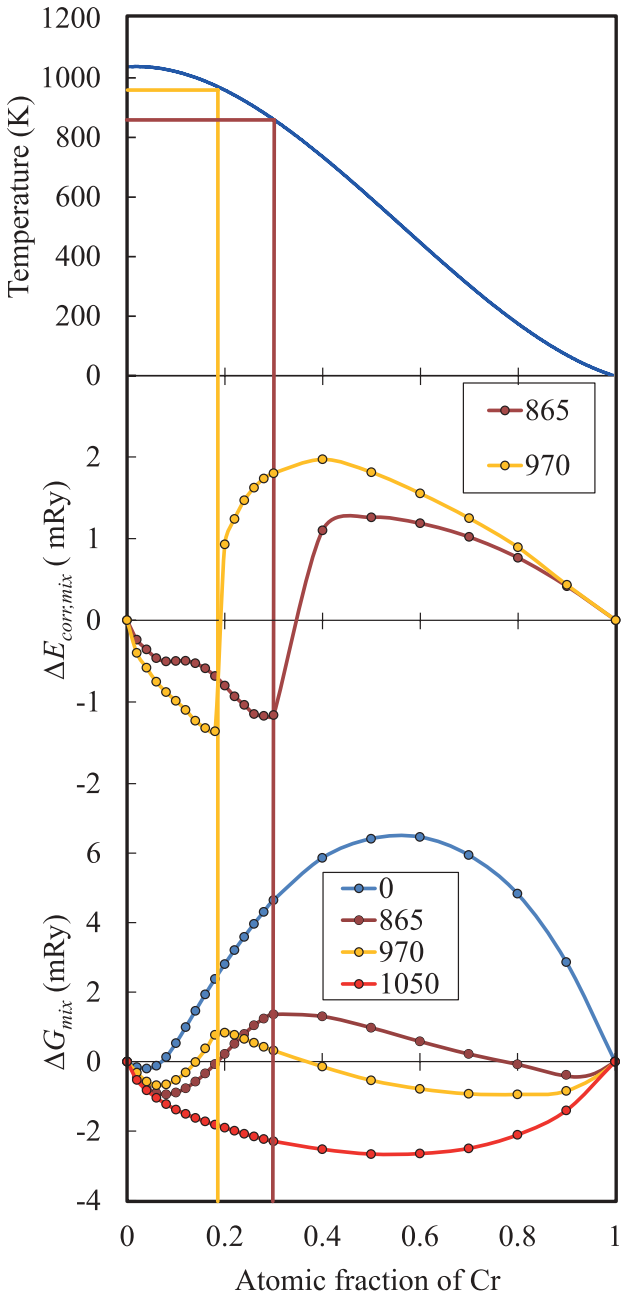


FIG. 16. (Color online) Gibbs free-energy of mixing for 865 and 970 K (bottom panel), energy correction due to the magnetic SRO (middle panel), and analytical fit for the Curie temperature used in the calculations (upper panel).

from other thermal excitations, for instance, from the thermal lattice expansion. Finally, the configurational entropy of a random alloy $S_{\text{conf}}(c)$ is

$$S_{\text{conf}}(c) = -k_B[c \ln c + (1-c)\ln(1-c)]. \qquad (21)$$

In the lower panel of Fig. 16 we show the mixing Gibbs free-energy $\Delta G(c,T)$ calculated for two different temperatures close to the Curie temperature of Fe. It has quite a peculiar form with pronounced minima and maxima in the Fe-rich region. The position of the maxima can be actually traced back to the point of the concentration where the magnetic phase transition

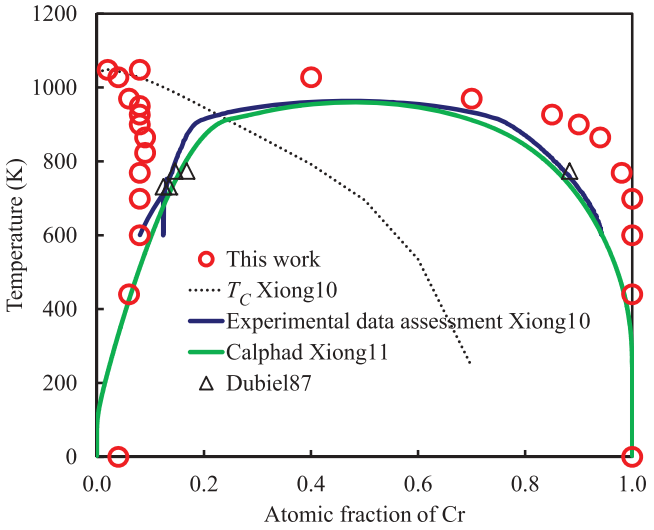


FIG. 17. (Color online) Fe-Cr bcc phase diagram.

happens at the corresponding temperature (upper panel of Fig. 16). In fact, in the absence of the magnetic SRO energy correction, the maximum would be much more pronounced with a pronounced peculiarity. This can be clearly seen from the magnetic SRO energy correction presented in the middle panel of the figure, which shows that it has a sharp minimum at the corresponding concentrations.

The calculated bcc Fe-Cr phase diagram for random alloys is shown in Fig. 17 together with the recent assessment of experimental data[3] and the corresponding results of CALPHAD modeling.[93] The experimental data by Dubeil and Inden[4] obtained after 4–11 years of annealing, are included in the figure as well. Considering the CALPHAD results to be an accurate fit to the experimentally available data, it is obvious that the present calculations underestimate the solubility of Cr and Fe in the temperature range of 700–800 K, which especially small in the case of the Fe solubility in Cr.

Let us note that our results for the solubility of Cr in Fe are in reasonable agreement with the small-angle neutron diffuse scattering study of neutron-irradiated Fe-Cr alloys at 573 K.[94] In this experiment the equilibrium in $Fe_{0.88}Cr_{0.12}$ and $Fe_{0.91}Cr_{0.09}$ alloys has been reached via irradiation-enhanced diffusion. Comparing the scattering cross section of the irradiated and unirradiated samples, it has been found that the solubility limit of Cr in bcc at 300 °C is 8.8%,[94] which is close to the present theoretical result 7%.

Another feature, which is much less pronounced in the phase diagram recently evaluated by the CALPHAD method, is the abnormal decrease in the solubility of Cr in Fe-rich alloys at high temperatures close to the magnetic phase transition. This feature, called sometimes a Nishizawa horn, has been thoroughly discussed for magnetic alloys by Nishizawa *et al.*[81,83,84] In this particular case, it results from a relative stabilization of Cr alloying in the ferromagnetic state compared to that in the paramagnetic in Fe-rich alloys up to 20 at.% Cr (see Fig. 3).

In our calculations the Nishizawa horn is deeply pronounced, and we find that it is a very stable feature, which cannot be significantly altered by tuning the mixing

free-energy. Of course, the present *ab initio* modeling of the phase equilibria in the bcc Fe-Cr alloys is quite approximate, especially at high temperatures. However, it is very difficult to see the origin of the problem.

The same concerns the quite restricted solubility of Cr in the temperature interval of 500–800 K. It is not clear how it can be corrected since the main force driving the phase separation in the Cr-rich Fe-Cr alloys is the very strong chemical interactions. It is very difficult to balance them by other contributions. In our view, more thorough theoretical and experimental investigations are needed to establish accurate phase diagram of Fe-Cr system.

## VIII. SUMMARY

The phase diagram of bcc Fe-Cr alloys has been calculated using a set of different models and approximations serving the purpose of getting the Gibbs free-energy of a system as a function of its composition and temperature. The main aim of this investigation has been, however, to keep as much input as possible from the-state-of-the-art first-principles calculations within DFT and, in particular, within the GGA or LSDA. Such a choice imposes, first of all, an obvious restriction on the truly *ab initio* inclusion of the temperature-induced magnetic excitations, which is an extremely difficult problem for this system due to the itinerant nature of magnetism.

Restricted by the GGA (or LSDA) we have had to decide first on the accuracy of those approximations for the magnetic energy, the subject of extreme importance for the first-principles modeling of Fe alloys, although it is almost never mentioned in the literature.[16] The difference of the magnetic energy deduced from the experimental heat capacity and GGA (LSDA) results is indeed huge, of about 7–8 mRy/atom. This is twice of the value of the experimental enthalpy of formation of Fe-Cr alloys in the paramagnetic state.

Our analysis, based on the classical Monte Carlo calculations of magnetic energy in the paramagnetic state, has demonstrated that this energy, which is due to the magnetic SRO effects, is quite large and its experimental underestimate could be the source for the discrepancy. We have also demonstrated that all the other properties related to the magnetic energy (the magnon spectrum, Curie temperature) are well reproduced by the LSDA, and therefore one can build a quantitatively accurate model for the magnetic free-energy based on the corresponding first-principles results for the total energies.

Such a model, which is based on the PDLM total energies, experimental data for the reduced magnetization and classical Monte Carlo simulations for the energy in the paramagnetic state, have been proposed in the present paper. Its main ingredient is the magnetic SRO energy correction, which allows one to eliminate the huge error in the DLM description due to the magnetic SRO. It is introduced consistently in a way to keep the whole magnetic energy, which is determined in the direct first-principles calculations, properly normalized. As has been shown, such a model leads to a substantial improvement of the agreement between the theoretical and experimental magnetic energies.

Another important check of the accuracy and reliability of the used first-principles techniques is the calculations of the effective pair interactions in Fe-Cr alloys as a function of concentration and temperature. First of all, we show that our PDLM model and first-principles techniques accurately reproduce the concentration dependence of the effective pair interactions in Fe-rich alloys in the FM state. Second, we calculate the effective pair interactions in the equiatomic Fe-Cr alloy in the paramagnetic state at 1100 K. These results are in good agreement with the available experimental data. Finally, we estimate the contribution from the ASRO to the free-energy and show that it is relatively small, and therefore consider only random alloys in our model calculations.

To calculate the vibrational contribution to the free-energy of alloy we proposed here a simple average force constant model, equivalent to the VCA. It is accurate in the case of dilute alloys, and it reproduces very well the existing experimental data.

The final free-energy of mixing, used in the phase diagram calculations, have included practically all the relevant contributions. One of the main assumptions is the neglect of the atomic SRO effects. However, it is very difficult to make everything consistent in this case due to the nontrivial character of magnetism in this system. Nevertheless, we believe that this error could be compensated by the contribution from the local lattice relaxation effects, which should be reduced with the inclusion of the atomic SRO.

The calculated phase diagram is relatively close to the one obtained in the CALPHAD modeling. The main difference is (1) for the solubility of Fe in Cr, which is extremely low in our calculations compared to the CALPHAD modeling and experimental data, and (2) for the existence of the Nishizawa horn, which is almost absent in the recent CALPHAD evaluation, but pronounced in our calculations.

As for the solubility of Fe in Cr, we do not know what could be the source of so large solubility in the experiment. Our calculations show that the phase separation tendency due to chemical interactions is very strong in the Cr-rich Fe-Cr alloys. It is very unlikely that other contributions, for instance, vibrational, can be that significant at temperatures of 600–800 K.

The experimental investigation of the Nishizawa horn in this temperature region is extremely difficult due to the precipitation of the $\sigma$ phase. Thus, more theoretical investigations are needed to solve this disagreement.

## ACKNOWLEDGMENTS

We would like to acknowledge, Dr. P. A. Korzhavyi, Professor J. Ågren, and Dr. J. Odqvist for helpful discussions and Dr. W. Xiong for providing the most recent CALPHAD data on Fe-Cr. Also, we want to thank Dr. S. G. Fries for the valuable comments on the manuscript. Computer resources for this study have been provided by the Swedish National Infrastructure for Computing (SNIC) and MATTER Network, at the National Supercomputer Center (NSC), Linköping. This work was performed within the VINNEX center Hero-m, financed by the Swedish Governmental Agency for Innovation Systems (VINNOVA), Swedish industry, and the Royal Institute of Technology (KTH). This work was partially supported by he Swedish Research Council (VR) and European Research Council (Grant No. 228074, ALPAM).

*razvsevol@yahoo.com


[1] I. Cook, Nat. Mater. **5**, 77 (2006).
[2] H. Okamoto, in *ASM Handbook: Volume 3: Alloy Phase Diagrams*, edited by H. Baker (ASM International, Materials Park, OH, 1991).
[3] W. Xiong, M. Selleby, Q. Chen, J. Odqvist, and Y. Du, Crit. Rev. Solid State Mater. Sci. **35**, 125 (2010).
[4] S. M. Dubiel and G. Inden, Z. Metallkd. **78**, 544 (1987).
[5] G. Bonny, R. C. Pasianot, L. Malerba, A. Caro, P. Olsson, and M. Yu. Lavrentiev, J. Nucl. Mater. **385**, 268 (2009).
[6] P. Olsson, J. Wallenius, C. Domain, K. Nordlund, and L. Malerba, Phys. Rev. B **72**, 214119 (2005).
[7] J. O. Andersson and B. Sundman, CALPHAD: Comput. Coupling Phase Diagrams Thermochem. **11**, 83 (1987).
[8] P. E. A. Turchi, L. Reinhard, and G. M. Stocks, Phys. Rev. B **50**, 15542 (1994).
[9] M. Yu. Lavrentiev, R. Drautz, D. Nguyen-Manh, T. P. C. Klaver, and S. L. Dudarev, Phys. Rev. B **75**, 014208 (2007).
[10] M. Yu. Lavrentiev, D. Nguyen-Manh, and S. L. Dudarev, Phys. Rev. B **81**, 184202 (2010).
[11] C. Zener, Trans. AIME **203**, 619 (1955).
[12] R. J. Weiss and K. J. Tauer, Phys. Rev. **102**, 1490 (1956).
[13] P. Olsson, I. Abrikosov, L. Vitos, and J. Wallenius, J. Nucl. Mater. **321**, 84 (2003).
[14] P. Olsson, I. A. Abrikosov, and J. Wallenius, Phys. Rev. B **73**, 104416 (2006).
[15] T. P. C. Klaver, R. Drautz, and M. W. Finnis, Phys. Rev. B **74**, 094435 (2006).
[16] P. A. Korzhavyi, A. V. Ruban, J. Odqvist, J.-O. Nilsson, and B. Johansson, Phys. Rev. B **79**, 054202 (2009).
[17] A. V. Ruban, P. A. Korzhavyi, and B. Johansson, Phys. Rev. B **77**, 094436 (2008).
[18] M. Hennnion, J. Phys. F **13**, 2351 (1983).
[19] I. Mirebeau, M. Hennion, and G. Parette, Phys. Rev. Lett. **53**, 687 (1984).
[20] I. Mirebeau and G. Parette, Phys. Rev. B **82**, 104203 (2010).
[21] L. Vitos, H. L. Skriver, B. Johansson, and J. Kollar, Comput. Mater. Sci. **18**, 24 (2000).
[22] L. Vitos, Phys. Rev. B **64**, 014107 (2001).
[23] L. Vitos, I. A. Abrikosov, and B. Johansson, Phys. Rev. Lett. **87**, 156401 (2001).
[24] L. Vitos, *Computational Quantum Mechanics for Materials Engineers* (Springer, London, 2007).
[25] P. Hohenberg and W. Kohn, Phys. Rev. **136**, B864 (1964).
[26] B. L. Györffy, Phys. Rev. B **5**, 2382 (1972).
[27] E. Kabliman, P. Blaha, K. Schwarz, A. V. Ruban, and B. Johansson, Phys. Rev. B **83**, 092201 (2011).
[28] V. I. Razumovskiy, A. V. Ruban, and P. A. Korzhavyi, Phys. Rev. B **84**, 024106 (2011).
[29] I. A. Abrikosov, A. M. N. Niklasson, S. I. Simak, B. Johansson, A. V. Ruban, and H. L. Skriver, Phys. Rev. Lett. **76**, 4203 (1996); I. A. Abrikosov, S. I. Simak, B. Johansson, A. V. Ruban, and H. L. Skriver, Phys. Rev. B **56**, 9319 (1997).
[30] O. E. Peil, A. V. Ruban, and B. Johansson, Phys. Rev. B **85**, 165140 (2012).
[31] A. V. Ruban and H. L. Skriver, Phys. Rev. B **66**, 024201 (2002); A. V. Ruban, S. I. Simak, P. A. Korzhavyi, and H. L. Skriver, *ibid.* **66**, 024202 (2002).
[32] J. P. Perdew, K. Burke, and M. Ernzerhof, Phys. Rev. Lett. **77**, 3865 (1996).
[33] H. J. Monkhorst and J. D. Pack, Phys. Rev. B **13**, 5188 (1972).
[34] B. L. Gyorffy, A. J. Pindor, G. M. Stocks, and H. Winter, J. Magn. Magn. Mater. **45**, 15 (1984).
[35] B. L. Gyorffy, A. J. Pindor, J. B. Staunton, G. M. Stocks, and H. Winter, J. Phys. F **15**, 1337 (1985).
[36] B. Drittler, N. Stefanou, S. Blugel, R. Zeller, and P. H. Dederichs, Phys. Rev. B **40**, 8203 (1989).
[37] P. E. Blöchl, Phys. Rev. B **50**, 17953 (1994).
[38] G. Kresse and D. Joubert, Phys. Rev. B **59**, 1758 (1999).
[39] G. Kresse and J. Hafner, Phys. Rev. B **47**, 558 (1993).
[40] G. Kresse and J. Hafner, Phys. Rev. B **49**, 14251 (1994).
[41] G. Kresse and J. Furthmuller, Phys. Rev. B **54**, 11169 (1996).
[42] G. Kresse, J. Furthmuller, and J. Hafner, Europhys. Lett. **32**, 729 (1995).
[43] D. Alfe, program available at http://chianti.geol.ucl.ac.uk/∼dario.
[44] D. Alfe, Comput. Phys. Commun. **180**, 2622 (2009).
[45] J. P. Perdew, K. Burke, and Y. Wang, Phys. Rev. B **54**, 16533 (1996).
[46] H. Zhang, B. Johansson, and L. Vitos, Phys. Rev. B **79**, 224201 (2009).
[47] G. D. Preston, Philos. Mag. **13**, 419 (1932).
[48] R. Kohlhaas, P. Dünner, and N. Schmitz-Pranghe, Z. Angew. Phys. **23**, 245 (1967).
[49] T. I. Babyuk, G. P. Kushta, and O. I. Rybailo, Izv. Vyssh. Uucheb. Zaved., Chern. Metall., No. 7, 126 (1974).
[50] V. V. Sumin, V. G. Simkin, S. G. Sheverev, M. V. Leont'eva-Smirnova, and V. M. Chernov, Phys. Met. Metallogr. **108**, 633 (2009).
[51] P. Haas, F. Tran, and P. Blaha, Phys. Rev. B **79**, 085104 (2009).
[52] W. T. Geng, Phys. Rev. B **68**, 233402 (2003).
[53] A. A. Mirzoev, M. M. Yalalov, and D. A. Mirzaev, Phys. Met. Metall. **97**, 336 (2004).
[54] A. E. Kissavos, S. I. Simak, P. Olsson, L. Vitos, and I. A. Abrikosov, Comput. Mater. Sci. **35**, 1 (2006).
[55] W. A. Dench, Trans. Faraday Soc. **59**, 1279 (1963).
[56] I. Malinsky and F. Claisse, J. Chem. Thermodyn. **5**, 615 (1973).
[57] A. Liechtenstein, M. I. Katsnelson, V. P. Antropov, and V. A. Gubanov, J. Magn. Magn. Mater. **67**, 65 (1987).
[58] S. V. Halilov, A. Y. Perlov, P. M. Oppeneer, and H. Eschrig, Europhys. Lett. **39**, 91 (1997).
[59] V. P. Antropov, B. N. Harmon, and A. N. Smrinov, J. Magn. Magn. Mater. **200**, 148 (1999).
[60] S. Shallcross, A. E. Kissavos, V. Meded, and A. V. Ruban, Phys. Rev. B **72**, 104437 (2005).
[61] A. V. Ruban, S. Shallcross, S. I. Simak, and H. L. Skriver, Phys. Rev. B **70**, 125115 (2004).
[62] A. V. Ruban, S. Khmelevskyi, P. Mohn, and B. Johansson, Phys. Rev. B **75**, 054402 (2007).
[63] A. I. Lichtenstein, M. I. Katsnelson, and G. Kotliar, Phys. Rev. Lett. **87**, 067205 (2001).
[64] I. Leonov, A. I. Poteryaev, V. I. Anisimov, and D. Vollhardt, Phys. Rev. Lett. **106**, 106405 (2011).
[65] F. Körmann, A. Dick, T. Hickel, and J. Neugebauer, Phys. Rev. B **81**, 134425 (2010).
[66] P. D. Desai, J. Chem. Ref. Data **15**, 967 (1986).
[67] S. V. Halilov, H. Eschrig, A. Y. Perlov, and P. M. Oppeneer, Phys. Rev. B **58**, 293 (1998).
[68] C. K. Loong, J. M. Carpenter, J. W. Lynn, R. A. Robinson, and H. A. Mook, J. Appl. Phys. **55**, 1895 (1984).

[69]The magnon heat capacity scales as $T^{3/2}$ at low temperatures, while CALPHAD model logarithmically. Nevertheless, the low temperature region is not important for phase equilibria above 500 K.
[70]J. Crangle and G. M. Goodman, Proc. R. Soc. London Ser. A **321**, 477 (1971).
[71]M. D. Kuzmin, Phys. Rev. Lett. **94**, 107204 (2005).
[72]The determined in this way magnetic energy consists of some other contributions, for instance, the change of the energy due to the thermal lattice expansion. Nevertheless, we will keep this terminology for simplicity.
[73]A discussion of the magnetic SRO in paramagnetic Fe in terms of spin-spin correlation functions can be found in N. M. Rosengaard and B. Johansson, Phys. Rev. B **55**, 14975 (1997).
[74]G. Inden, Physica B+C **103**, 82 (1981).
[75]L. Reinhard, J. L. Robertson, S. C. Moss, G. E. Ice, P. Zschack, and C. J. Sparks, Phys. Rev. B **45**, 2662 (1992).
[76]F. Ducastelle and F. Gautier, J. Phys. F **6**, 2039 (1976).
[77]F. Ducastelle, *Order and Phase Stability in Alloys* (North-Holland, Amsterdam, 1991).
[78]It is easy to show that the energy of the atomic SRO is proportional to $c^2$, where $c$ is the concentration of minority alloy component. This means that it decreases very fast when concentration deviates from the equiatomic composition.
[79]R. V. Chepulskii, Phys. Rev. B **69**, 134431 (2004).
[80]F. Adcock, J. Iron Steel Inst. London **124**, 99 (1931).
[81]T. Nishizawa, M. Ko, and M. Hasebe, Acta Metall. **27**, 817 (1979).
[82]E. Fawcett, H. L. Alberts, V. Yu. Galkin, D. R. Noakes, and J. V. Yakhmi, Rev. Mod. Phys. **66**, 25 (1994).
[83]T. Nishizawa, S. M. Hao, M. Hasebe, and K. Ishida, Acta Metall. **31**, 1403 (1983).
[84]T. Nishizawa, J. Phase Equilib. **16**, 379 (1995).
[85]G. Ceder and A. van de Walle, Rev. Mod. Phys. **74**, 11 (2002).
[86]S. Ghosh, P. L. Leath, and M. H. Cohen, Phys. Rev. B **66**, 214206 (2002).
[87]A. Alam and A. Mookerjee, Phys. Rev. B **69**, 024205 (2004).
[88]A. Alam, R. K. Chouhan, and A. Mookerjee, Phys. Rev. B **83**, 054201 (2011).
[89]G. Grimvall, *Thermophysical Properties of Materials* (North-Holland, Amsterdam, 1986).
[90]M. S. Lucas, M. Kresch, R. Stevens, and B. Fultz, Phys. Rev. B **77**, 184303 (2008).
[91]B. Fultz, L. Anthony, J. L. Robertson, R. M. Nicklow, S. Spooner, and M. Mostoller, Phys. Rev. B **52**, 3280 (1995).
[92]V. L. Moruzzi, J. F. Janak, and K. Schwarz, Phys. Rev. B **37**, 790 (1988).
[93]W. Xiong, P. Hedström, M. Selleby, J. Odqvist, M. Thuvander, and Q. Chen, CALPHAD **35**, 355 (2011).
[94]F. Bergner, A. Ulbricht, and C. Heintze, Scr. Mater. **61**, 1060 (2009).